

# Lawrence Berkeley National Laboratory

## Recent Work

### Title

THE CLUSTER VARIATION METHOD AND THE CALCULATION OF ALLOY PHASE DIAGRAMS

### Permalink

<https://escholarship.org/uc/item/5dq5s5jh>

### Author

Fontaine, D. de.

### Publication Date

1988-02-01



# Lawrence Berkeley Laboratory

UNIVERSITY OF CALIFORNIA

## Materials & Chemical Sciences Division

RECEIVED  
LAWRENCE  
BERKELEY LABORATORY

JUN 9 1988

Presented at the NATO Advanced Study Institute  
on Alloy Phase Stability, Maleme, Crete,  
June 13-27, 1987

LIBRARY AND  
DOCUMENTS SECTION

### The Cluster Variation Method and the Calculation of Alloy Phase Diagrams

D. de Fontaine

February 1988

**TWO-WEEK LOAN COPY**

*This is a Library Circulating Copy  
which may be borrowed for two weeks.*



LBL-24934  
c.2

## **DISCLAIMER**

This document was prepared as an account of work sponsored by the United States Government. While this document is believed to contain correct information, neither the United States Government nor any agency thereof, nor the Regents of the University of California, nor any of their employees, makes any warranty, express or implied, or assumes any legal responsibility for the accuracy, completeness, or usefulness of any information, apparatus, product, or process disclosed, or represents that its use would not infringe privately owned rights. Reference herein to any specific commercial product, process, or service by its trade name, trademark, manufacturer, or otherwise, does not necessarily constitute or imply its endorsement, recommendation, or favoring by the United States Government or any agency thereof, or the Regents of the University of California. The views and opinions of authors expressed herein do not necessarily state or reflect those of the United States Government or any agency thereof or the Regents of the University of California.

**THE CLUSTER VARIATION METHOD AND THE CALCULATION OF ALLOY  
PHASE DIAGRAMS**

by

**D. de Fontaine**

Materials and Chemical Sciences Division  
Lawrence Berkeley Laboratory  
and  
Department of Materials Science and  
Mineral Engineering  
University of California  
Berkeley, CA 94720

February 1988

This work was supported by a grant from the Director, Office of Energy Research, Materials Sciences Division, U.S. Department of Energy, under contract DE-AC03-76SF00098.

# THE CLUSTER VARIATION METHOD AND THE CALCULATION OF ALLOY PHASE DIAGRAMS

D. de FONTAINE

University of California, Dept. of Materials Science and Mineral Engineering; and  
Lawrence Berkeley Laboratory, Berkeley, CA 94720

## 1. INTRODUCTION

I was asked by the Workshop organizers to write a tutorial on the Cluster Variation Method (CVM) in phase diagram calculations. Hence I shall present an elementary treatment of the essential features of the method rather than a comprehensive review.

As is well known, the CVM was originally proposed by Kikuchi<sup>1</sup> in 1951 as a hierarchy of approximation for the Ising model, in principle, in an arbitrary number of dimensions. The basic idea consists of handling local order as accurately as possible, then of expressing the configurational entropy in terms of small cluster probabilities. The corresponding free energy is then minimized with respect to independent configuration (cluster) variables. Higher cluster correlations are essentially treated by a superposition approximation. Hence, in the limit, the CVM is a classical theory. Much of the early work in the field was devoted by Kikuchi and collaborators to a systematic comparison of different levels of cluster approximations with known exact solutions such as that of Onsager's solution of the two-dimensional Ising model in zero field. In favorable cases, the CVM transition temperature turned out to be very close to the exact one. Unfortunately, the CVM being a classical theory, predicts critical exponents with classical values. That fact tended to discredit the CVM in the eyes of critical phenomena specialists.

Kikuchi's original approach to deriving CVM entropy formulas for various lattices and cluster approximations was an essentially geometrical one. Soon, however, other, more analytical (and simpler) methods appeared, those of Barker<sup>2</sup> and of Hijmans and de Boer<sup>3</sup>. Later, a very general and systematic method was developed by Sanchez<sup>4-6</sup>. This method, based on the idea of expressing the CVM free energy in terms of linearly independent correlation functions, is the most widely used today; it will be reviewed in this article.

A convenient method of minimizing the CVM free energy is the Natural Iteration Method, also developed by Kikuchi<sup>7</sup>. It was proposed just after Van Baal<sup>8</sup> had demonstrated the use of the CVM in the calculation of temperature/composition phase diagrams for binary alloys. Subsequently it was shown that Van Baal's ideas could be used to produce a rather faithful approximation to the crystalline equilibria in the Cu-Au phase diagram<sup>9,10</sup>.

Because of its importance for alloy thermodynamics, development of the CVM is being pursued very actively in both theoretical and practical aspects. The most general and sophisticated formulation of the method is that developed initially independently by Sanchez and by Ducastelle and presented in a joint publication<sup>11</sup>. The present description is a simplified version of this approach. Recently, significant progress has been made in the derivation of suitable criteria for the selection of clusters<sup>12,13</sup>. Finel presented the essence of his method at the Workshop; a complete description thereof can be found in

Finel's Doctoral Dissertation<sup>13</sup> which contains the most complete description of the CVM known to me.

The present article is divided into three main sections: the first one is a fairly detailed exposition of the CVM basics, the second one describes stability analysis, and the third one summarizes a recent application of the CVM to phase diagram calculations. A two-dimensional example will be worked out in some detail. The two-dimensional geometry is of course much simpler to visualize than the three-dimensional, also, the example chosen is relevant to the currently hot topic of vacancy ordering in the high- $T_C$  superconductor  $YBa_2Cu_3O_x$  ( $6 < x < 7$ ).

## 2. THE CVM FORMALISM

Calculations of properties of pure elements and stoichiometric compounds has progressed considerably in recent years, but it is clear that alloys (mixtures of one or more elements) present additional difficulties. Pure crystals or compounds can be uniquely described by their unit cells, and completely disordered solid solutions can be described by specifying the average lattice and the average composition. For phase equilibrium calculations, however, it is essential to consider *states of partial order*: arbitrary degrees of long-range order (LRO), with short-range order (SRO) present as well.

Hence, the study of alloy thermodynamics must begin by an adequate description of the state of order (Sect. 2.1). Then, it is necessary to derive a statistical model, given that the statistical thermodynamics of three dimensional systems cannot be treated exactly. In particular, what is needed is an approximate but reliable expression for the configurational entropy (Sect. 2.2). Thirdly, the thermodynamics of the system must be completed by introducing physical parameters, the so-called effective cluster interactions which must be determined either empirically or by quantum mechanical calculations (Sect. 2.3).

### 2.1. State of Order

I shall now summarize, in simplified form, the elegant CVM treatment of Sanchez, Ducastelle and Gratias<sup>11</sup> (SDG). These authors show that the CVM actually provides a completely general and optimal way of describing partial order, the basic idea being that of representing local order by sampling configurational space by means of small clusters of crystal lattice sites. This is accomplished by expressing arbitrary functions of configuration in terms of a complete set of orthonormal functions.

In SDG, multicomponent systems were considered. Here, for simplicity, only binary systems will be treated. Each lattice site ( $p$ ) can then be occupied by either an A or a B atom, with corresponding "spin" variable  $\sigma_p = +1$  or  $-1$ . The complete crystal, of  $N$  sites, has instantaneous configuration fully specified by the vector  $\sigma = (\sigma_1, \sigma_2, \dots, \sigma_N)$ . The scalar product of two functions of configuration,  $f(\sigma)$  and  $g(\sigma)$ , is defined as

$$\langle f, g \rangle = \rho_N \text{Tr}^{(N)} f \cdot g \quad (1)$$

where the "trace" operation is defined as a sum over all configurations

$$\text{Tr}^{(N)} = \sum_{\sigma_1 = \pm 1} \sum_{\sigma_2 = \pm 1} \cdots \sum_{\sigma_N = \pm 1} \quad (2)$$

with normalization

$$\rho_N = 2^{-N}$$

The scalar product definition (1) allows the construction of a complete orthonormal set (CONS) of functions. For a single lattice point, the set of functions is simply

$$\Gamma(\sigma_p) = \{\Gamma_0, \Gamma_1\} = \{1, \sigma_p\} \quad (3)$$

such that

$$\langle \Gamma_i(\sigma_p), \Gamma_j(\sigma_p) \rangle = \delta_{ij} \quad (4)$$

where the Kronecker delta is unity if  $i=j$ , zero otherwise. Now form the direct product, over all  $N$  lattice sites,

$$\Gamma(\sigma_1) \times \Gamma(\sigma_2) \times \dots \times \Gamma(\sigma_N) = \Phi \quad (5)$$

By (5), each function of the set  $\Phi$ , except  $\Phi_0=1$ , is itself a product

$$\Phi_\alpha = \sigma_{p_1} \sigma_{p_2} \dots \sigma_{p_n}$$

over the cluster  $\sigma = \{p_1, p_2, \dots, p_n\}$  of  $n$  points. From (1) and (2) we then have

$$\langle \Phi_\alpha, \Phi_\beta \rangle = \delta_{\alpha\beta} \quad (6)$$

and the closure relation

$$\rho_N \sum_{\beta} \Phi_{\beta}(\sigma) \Phi_{\beta}(\sigma') = \delta_{\sigma, \sigma'} \quad (7)$$

Hence, by (4) and (7) the set  $\Phi$  is a CONS. It is convenient to treat separately the configuration independent function  $\Phi_0=1$ . Then any function may be expanded as

$$g(\sigma) = g_0 + \sum_{\alpha} g_{\alpha} \Phi_{\alpha}(\sigma) \quad (8)$$

with

$$g_0 = \langle 1, g \rangle, \quad g_{\alpha} = \langle \Phi_{\alpha}, g \rangle \quad (9)$$

For example, the Ising Hamiltonian may be expanded in terms of *cluster functions*  $\Phi_{\alpha}$  as follows

$$H = \sum_{\alpha} V_{\alpha} \Phi_{\alpha} \quad (10)$$

where the  $V_{\alpha}$  are *cluster interactions* defined by

$$V_{\alpha} = \langle \Phi_{\alpha}, H \rangle \quad (11)$$

To evaluate averages, it is necessary to define a configuration density thus

$$\rho(\sigma) = Z^{-1} e^{-H/k_B T} \quad (12)$$

with partition function

$$Z = \text{Tr}^{(N)} e^{-H/k_B T} \quad (13)$$

where  $k_B T$  has its usual meaning. The density can also be expanded in orthonormal functions

$$\rho(\sigma) = \rho_N^{\circ} [ 1 + \sum_{\alpha} \Phi_{\alpha}(\sigma) \xi_{\alpha} ] \quad (14)$$

where  $\xi_{\alpha}$  is a *multiplet correlation* function for cluster  $\alpha$ , defined as the average value of the product of  $\sigma$  variables over the cluster  $\alpha$

$$\xi_{\alpha} = \langle \Phi_{\alpha}, \rho \rangle = \rho_N^{\circ} \langle \Phi_{\alpha} \rangle \quad (15)$$

It is also useful to consider *reduced densities* obtained by performing the partial trace

$$\rho_{\beta} = \text{Tr}^{(N-\beta)} \rho \quad , \quad (16)$$

i.e. by summing over all configurations except that,  $\sigma_{\beta}$ , of the  $n$ -point cluster  $\beta$  envisaged. The partial trace operating on  $\Phi_{\alpha}$  in (14) equals  $(1/\rho_{\beta}^{\circ})\Phi_{\alpha}$  if  $\alpha$  is contained in  $\beta$  ( $\beta \supset \alpha$ ) and zero otherwise, where  $1/\rho_{\beta}^{\circ} = 2^n$ . The reduced density can be regarded as the expectation value, in an ensemble of systems, of the cluster  $\alpha$  having configuration  $\sigma_{\beta}$ . Thus,  $\rho_p(\sigma_p)$  is simply the average concentration of A ( $\sigma_p = +1$ ) or B ( $\sigma_p = -1$ ) atoms, at site  $p$ , over the ensemble. If all lattice points  $p$  are equivalent, then  $\rho_p$  is the crystal average. If long-range order is present, distinct sub-lattices must be defined, and averages taken only over points of a given sublattice,  $p_i$ , say. By combining Eqs. (14) and (16) we then have, for cluster concentrations, or reduced densities, expressed in terms of correlations functions,

$$\rho_{\beta}(\sigma_{\beta}) = \rho_{\beta}^{\circ} [ 1 + \sum_{\alpha < \beta} \Phi_{\alpha}(\sigma_{\beta}) \xi_{\alpha} ] \quad , \quad (17)$$

where the summation is over all subclusters ( $\alpha$ ) of the cluster  $\alpha$ . This important formula was first derived by Sanchez<sup>4</sup>. The notion of partial trace was introduced into the CVM by Morita<sup>14</sup>. In practice, it is convenient to group all  $\xi_{\alpha}$  which are identical because of the symmetry of the crystal structure. Equations (14) or (17) then take on a slightly different form, with appropriate sums of  $\Phi_{\alpha}$  functions being regarded as elements of the so-called *configuration matrix* [see Eqs. (67) and (68), below]. The crystallography of the problem is thus introduced into the statistical formulation by means of this matrix.

## 2.2. Cluster Statistics

The energy and configurational entropy can be written as, respectively,

$$E[\rho] = \text{Tr}^{(N)} \rho H \quad (18)$$

and

$$S[\rho] = -k_B \text{Tr}^{(N)} \rho \ln \rho \quad (19)$$

The free energy is then given by

$$F[\rho] = \text{Tr}^{(N)} \rho [H + k_B T \ln \rho] \quad (20)$$



E, S and F are to be regarded as functionals in  $\rho(\sigma)$ , and will take on their equilibrium (expectation) values if  $\rho$  corresponds to the correct equilibrium distribution of configurations. In traditional variational treatments,  $F[\rho]$  is minimized with respect to  $\rho$  subject to the constraint  $\text{Tr } \rho = 1$ . It was shown by SDG<sup>11</sup>, however, that the equilibrium free energy could be obtained by a purely algebraic procedure, as will now be demonstrated. In a sense, the "Variation" has now been taken out of the variational treatment. It is, of course, impossible to consider the full density function  $\rho(\sigma)$  over all configurations on all lattice sites. Hence, some method must be devised for handling only a small number of configurations. In the CVM, this is accomplished by considering configurations over a small number of small clusters, up to some maximum-size cluster(s). Usually, the larger the clusters retained, the better will be the approximation to the free energy.

In the energy expression, the approximation consists of neglecting interaction energies  $V_\alpha$  in Eq. (10) for all clusters not contained in the maximal cluster. The same simple procedure will not do for the entropy expression, however: the  $\ln \rho$  term cannot be written as a truncated sum of partial densities of the type (16), as no convergence is expected. Instead, following Morita<sup>14</sup>, we define new functions  $\tilde{\rho}_\beta$  by writing successively

$$\rho_1 = \tilde{\rho}_1 \quad , \quad \rho_{12} = \tilde{\rho}_1 \tilde{\rho}_2 \tilde{\rho}_{12} \quad , \quad \dots \quad \rho_\alpha = \prod_{\beta < \alpha} \tilde{\rho}_\beta \quad , \quad \dots$$

with, finally

$$\rho = \prod_{\alpha} \tilde{\rho}_\alpha \quad (21)$$

The CVM approximation consists in truncating the product (21), by assuming that the cumulant corrections  $\tilde{\rho}_\gamma$  for  $\gamma$  not contained in the maximal cluster are equal to unity. Hence,

$$\ln \tilde{\rho} = \sum'_{\beta} \ln \tilde{\rho}_\beta \quad (22)$$

the accent on the summation denoting a truncated sum. It is now necessary to relate the  $\ln \tilde{\rho}_\beta (= \Omega_\beta$ , say) to  $\ln \rho_\alpha (= \Lambda_\alpha$ , say) which can be done by procedures already developed by Barker<sup>2</sup> and Hijmans and de Boer<sup>3</sup>. To this end, we write Eq. (22) as a sum over the  $\Lambda_\alpha$  times some coefficients  $a_\alpha$ , determined only by geometrical considerations:

$$\sum'_{\beta} \Omega_\beta = \sum'_{\alpha} a_\alpha \Lambda_\alpha = \sum'_{\alpha} a_\alpha \sum_{\beta < \alpha} \Omega_\beta = \sum'_{\beta} \left( \sum_{\alpha \supset \beta} a_\alpha \right) \Omega_\beta \quad (23)$$

Therefore,

$$\sum_{\alpha \supset \beta} a_\alpha = 1 \quad , \quad (24)$$

there being a separate Eq. (24) for each subcluster  $\alpha$  contained in the set of maximal clusters. Thus, the  $a_\alpha$  can be determined uniquely by recursion.

We have therefore derived an important expression

$$\ln \rho = \sum_{\alpha} a_{\alpha} \ln \rho_{\alpha} \quad (25)$$

whereby the logarithm of the density function is approximated by a weighted sum or reduced densities, i.e. cluster concentrations. By taking the logarithm of both sides of Eq. (12) we have

$$\ln \rho = -\ln Z - \frac{H}{k_B T}$$

or, using (25),

$$k_B T \sum_{\alpha} a_{\alpha} \ln \rho_{\alpha} = (-k_B T \ln Z) \Phi_0 - \sum_{\beta} V_{\beta} \Phi_{\beta}$$

By properties of the CONS we therefore have, as in Eq. (9):

$$-k_B T \ln Z = Z \langle 1, \sum_{\alpha} a_{\alpha} \ln \rho_{\alpha} \rangle \quad (26)$$

and

$$-V_{\beta} = Z \langle \Phi_{\beta}, \sum_{\alpha} a_{\alpha} \ln \rho_{\alpha} \rangle \quad (27)$$

the latter equation can be rewritten as

$$V_{\beta} = \sum_{\alpha \supset \beta} a_{\alpha} \rho_{\alpha} \text{Tr}^{(\alpha)} \Phi_{\beta} \ln \rho_{\alpha} \quad (28)$$

which is exactly the result which would have been obtained by direct minimization of the free energy with respect to the correlation functions  $\xi_{\beta}$ . In the Eqs. (28), the  $\rho_{\alpha}$  must be replaced by their expressions in terms of the independent variables  $\xi_{\beta}$ . There results a set of non-linear equations in as many unknowns as there are maximal clusters and their distinct subclusters. Solving this set of equations by numerical techniques constitutes a major difficulty of the CVM, hence, in practice, clusters must be kept small and few in number.

By a well-known result of statistical mechanics, Eq. (26) gives directly the equilibrium free energy:

$$F = k_B T \sum_{\alpha} a_{\alpha} \text{Tr}^{(\alpha)} \ln \rho_{\alpha} \quad (29)$$

The free energy functional itself is, from Eqs. (20), (10), (15) and (25),

$$F[\rho] = \sum_{\beta} V_{\beta} \xi_{\beta} + k_B T \sum_{\alpha} a_{\alpha} \text{Tr}^{(\alpha)} \rho_{\alpha} \ln \rho_{\alpha} \quad (30)$$

which is the classical CVM expression for the free energy. Note that the two sums in Eq. (30) need not run over the same clusters; it is only required that the entropy sum contain the maximal cluster(s), and the energy sum include only clusters contained in the maximal one(s). Of course, some of the  $a_{\alpha}$  subclusters may vanish, as explained by SDG.

### 2.3. Internal Energy

In order to calculate phase diagrams, it is not sufficient to treat Ising models alone: it is required to evaluate cohesive energies of various phases, in various states of order, referred to the same reference energy, for instance the energy of an infinitely dilute gas of pure A and pure B atoms,  $E_A^\infty$  and  $E_B^\infty$ , say.  $E_A^\alpha$  and  $E_B^\alpha$  are then the cohesive energies of pure A and B in the  $\alpha$  phase and  $E_A^\beta$  and  $E_B^\beta$  are the corresponding cohesive energies in the  $\beta$  phase. Actually, the cohesive energy  $E_{dis}$  of random mixtures of A and B, in  $\alpha$  or  $\beta$  as a function of concentration  $c$  of B atoms, will differ from the linear interpolation by amount  $\Delta E_{dis}$  the energy of completely random mixing.

It is possible to use the concepts derived in Sects. 2.1 and 2.2 to obtain formal expressions for the physical energy parameters required. To that end, let  $E(\sigma)$  denote the cohesive energy of a particular configuration ( $\sigma$ ), on a given lattice ( $\alpha, \beta, \dots$ ). The expectation value of  $E$ , for distribution  $\rho$ , will be

$$\langle E \rangle = \text{Tr}^{(N)} \rho(\sigma) E(\sigma) \quad (31)$$

Inserting expression (14) for the density  $\rho$  into (31) then yields

$$\langle E \rangle = E_0 + \sum_{\alpha} E_{\alpha} \xi_{\alpha} \quad (32)$$

with

$$E_0 = \rho_{\alpha}^0 \text{Tr}^{(N)} E(\sigma) \quad (33)$$

and

$$E_{\alpha} = \langle \Phi_{\omega} E \rangle = \rho_N^0 \text{Tr}^{(N)} \Phi_{\alpha}(\sigma) E(\sigma) \quad (34)$$

Note that, in this *grand canonical averaging*, because of the Trace operation, the energy  $E_0$  and the effective cluster interactions  $E_{\alpha}$  are not only configuration independent but even concentration independent.

Let us rewrite (34) explicitly for the case of pair interactions  $E_r$ , where  $r$  denotes the spacing between lattice points  $p$  and  $q$  of the pair:

$$V_r \equiv E_{pq} = \frac{1}{2} \sum_{\sigma_p = \pm 1} \sum_{\sigma_q = \pm 1} \sigma_p \sigma_q \frac{1}{2^{N-2}} \text{Tr}^{(N-2)} E(\sigma) \quad (35)$$

where the trace operation is carried out everywhere except at  $p$  and  $q$ . From Eq. (35) follow the definition of *Effective Pair Interactions* (EPI):

$$V_r \equiv \frac{1}{4} (V_{AA} - V_{AB} - V_{BA} + V_{BB}) \quad (36)$$

where  $V_{ij}$  ( $i, j = A, B$ ) represents the energy of the  $r^{\text{th}}$  ( $i, j$ ) pair embedded in an artificial medium in which all configurations are equally represented.

Unfortunately, Eqs. (34) or (35) cannot be used to calculate the cluster interactions since the configuration energies  $E(\sigma)$  are, of course, not known. Hence, a more direct method of computation for the  $E_{\alpha}$  is required. It has been argued<sup>15,16</sup> that the proper way to calculate effective cluster interactions is by means of a perturbation expansion of a disordered medium of specified concentration  $c$ . It appears that the expansion is much

more rapidly convergent if the states of (partial) order are considered as perturbations of the disordered states rather than as perturbations of the pure states or their linear interpolations. Quantum mechanical techniques suitable for performing such calculations are now available. For now, let us merely show how Eqs. (31) to (35) must be modified formally in order to obtain disordered state energies and concentration dependent cluster interactions.

In a sample containing a large number  $N$  of atoms, it is expected that, at equilibrium, the concentration  $c$  of the systems in a grand canonical ensemble will hardly ever depart significantly from the equilibrium concentration  $c^\circ$ . In other words, the density function  $\rho(\sigma)$  will be very sharply peaked about configurations having average concentration  $c^\circ$ . Hence, in Eq. (31), it is practically equivalent to sum only over those configurations  $\{\sigma^\circ\}$  which all have concentration  $\sigma^\circ$ :

$$\langle E \rangle \equiv \text{Tr}^{(N)} \rho(\sigma^\circ) E(\sigma^\circ) \quad (37)$$

where the superscript  $(\circ)$  denotes *canonical averaging*, as it were. We now have

$$\langle E \rangle = E_o^\circ + \sum_{\alpha} E_{\alpha}^{\circ} \xi_{\alpha} \quad (38)$$

with

$$E_o^\circ = \rho_N^\circ \text{Tr}^{(N)} E(\sigma^\circ) \quad (39)$$

and

$$E_{\alpha}^{\circ} = \rho_N^\circ \text{Tr}^{(N)} \Phi(\sigma^\circ) E(\sigma^\circ) \quad (40)$$

The total number of configurations having fixed number  $(N_A, N_B)$  of A and B atoms is

$$M = \frac{N!}{N_A! N_B!} \quad (41)$$

so that the energy of the completely random state of concentration  $c^\circ = N_B/(N_A + N_B)$  is, by Eq. (38),

$$E_{\text{dis}} = \frac{1}{M} \text{Tr}^{(N)} E(\sigma^\circ) = E_o^\circ + \sum_{\alpha} E_{\alpha}^{\circ} \xi_{\alpha}^R \quad (42)$$

where  $\xi_{\alpha}^R$  denote multiplet correlation functions in the fully disordered state. It is now apparent that the disordered energy  $E_{\text{dis}}$  and the cluster interactions  $E_{\alpha}^{\circ}$  are concentration dependent since, in Eqs. (40) and (42), the Trace operation samples different configurations at each concentration  $c$ .

The term  $E_{\alpha}^{\circ}$  may be eliminated from Eq. (38) by means of Eq. (42):

$$\langle E \rangle = E_{\text{dis}} + E_{\text{ord}} \quad (43)$$

where the disordered state energy  $E_{\text{dis}}$  is the energy of the completely disordered medium, in a given crystal structure, calculated in a single-site coherent potential approximation (CPA), for instance, and  $E_{\text{ord}}$  is given by

$$E_{\text{ord}} = \sum_{\alpha} E_{\alpha}^{\circ} \delta \xi_{\alpha} \quad (44)$$

where

$$\delta \xi_{\alpha} = \xi_{\alpha} - (\xi_1)^n \quad (45)$$

since the correlation function, in the fully disordered state, for an  $\alpha$  cluster of  $n$  points is practically equal to  $n^{\text{th}}$  power of the point correlation function  $\xi_1 = c_A - c_B = 1 - 2c$ . The accent on the summation in Eq. (44) indicates that, because of Eq. (45), the point clusters are not included in the sum. Eqs. (43) to (45) were given previously by Sigli and Sanchez<sup>17</sup>. The  $E_{\alpha}$ , or  $V_{\alpha}$  in the notation of previous Sections, must now be calculated. This can be accomplished by perturbing the single site CPA according to the so-called Generalized Perturbation Method (GPM)<sup>15,16</sup>. Alternately, the Embedded Cluster Method<sup>18</sup> may be used since, by Eq. (40), each cluster interaction  $V_{ij}$  in Eq. (36), rewritten for canonical averaging, as in Eq. (40), represents the energy of cluster  $\alpha$  embedded in a medium of random configuration of concentration  $c$ .

The derivations given above may explain formally why pair interactions  $E_r$ , for large spacing  $r$ , tend to become small in magnitude: at large spacing in a random medium,  $V_{ij}$  is approximately given by the sum of point energies  $V_i + V_j$ , hence the linear combination  $V_{AA} + V_{BB} - 2V_{AB}$  will tend to vanish.

To complete the calculation of the internal energy,  $E_{\text{ord}}$  must be evaluated, which requires, in addition to the  $E_{\alpha}^{\circ}$ , knowledge of the equilibrium correlation functions  $\xi_{\alpha}$ . These must be obtained by minimizing the free energy, at given temperature and concentration, by solving the system of algebraic equations (28). In summary, then,  $E_{\text{dis}}$  and  $E_{\alpha}^{\circ}$  (or  $V_{\alpha}$ ) can all be calculated by Quantum Mechanical methods at absolute zero of temperature. The  $\xi_{\alpha}$  are calculated by the CVM with temperature independent parameters. Hence, the procedure described here achieves a very convenient decoupling of the Quantum and Statistical Mechanical computations.

The determination of alloy phase equilibrium in the CVM framework will be deferred to Sect. 4. Before that, it is necessary to discuss the topic of configurational stability (Sect. 3).

### 3. STABILITY

#### 3.1. Susceptibility

Stability theory is concerned with the response of a system to a small applied field, in the present case, a "configurational" field, created by appropriate chemical potential changes. Since such responses are best expressed in reciprocal, or  $k$ -space, formalism, it is advantageous to modify the cluster notation used up to now. For that purpose, we specify a cluster  $\alpha$  by its type  $q$  and by the point  $p$  at which it is located:  $\alpha \rightarrow q, p$ . Equation (30) can now be expanded in powers of linearly independent cluster correlation functions  $\xi_{q(p)}$ :

$$F = F_0 + F_1 + F_2 + \dots \quad (46)$$

where each term groups like power of  $\xi$ . Stability analysis considers only small variation  $\delta \xi$  so that the Taylor's expansion (46) may be terminated at the second-order term. Since

$F_1$  vanishes at equilibrium, a small variation about the unperturbed state may be expressed as the quadratic form

$$\delta F = F_2 = \frac{N}{2} \sum_{qq'} \sum_{pp'} f_{qq'}(p, p') \delta \xi_q(p) \delta \xi_{q'}(p')$$

where  $F_{qq'}$  is the second derivative with respect to  $\xi_q \xi_{q'}$ , at the indicated points, of the free energy per unit cell. Because of translational symmetry in the disordered (unvaried) state,  $f_{qq'}$  is a function of the distance between  $p$  and  $p'$  only.

A first diagonalization is accomplished by Fourier transforming over space:

$$\delta F = \frac{N^2}{2} \sum_{qq'} F_{qq'}(\mathbf{k}) \delta X_q(\mathbf{k}) \delta X_{q'}(\mathbf{k}) \quad (47)$$

where  $F_{qq'}$  and  $X_q$  are, respectively, the Fourier transforms of  $f_{qq'}(p'-p)$  and  $\xi_q(p)$ . Expression (47) may be further diagonalized in cluster space:

$$\delta F = \frac{N^2}{2} \sum_q \Lambda_q(\mathbf{k}) |\delta Y_q(\mathbf{k})|^2 \quad (48)$$

where  $\Lambda_q$  denotes the eigenvalues of the Hermitian matrix  $F$  and  $Y_q$  are normal "cluster modes".

The system is unconditionally stable if  $\delta F$  is positive for all possible configurational variations i.e., if all eigenvalues  $\Lambda$  are positive, or equivalently if the matrix  $F$  is positive definite. Instability sets in for given  $\mathbf{k}$  when the determinant of  $F$  vanishes

$$\text{Det} [F(\mathbf{k})] = 0 \quad (49)$$

The matrix  $F$  is a function of temperature and concentration, so that, for each possible wave vector  $\mathbf{k}$ , condition (49) represents a locus in phase diagram space. The locus lying at highest temperature will correspond to a particular wave vector  $\mathbf{k}_0$ , that of the *ordering wave*.

Above the highest stability limit, a generalized susceptibility  $\chi_{qq'}(\mathbf{k})$  may be defined as the expectation value of the product of two cluster waves

$$\chi_{qq'}(\mathbf{k}) = \langle \chi_q(\mathbf{k}) \chi_{q'}(\mathbf{k}) \rangle = N k_B T G_{qq'}(\mathbf{k}) \quad (50)$$

where the star denotes a complex conjugate quantity and  $G_{qq'}$  is the  $qq'$  element of the matrix  $F^{-1}$ , the inverse of the second derivative matrix.

So-called short-range order intensity  $I_{SRO}$ , in appropriate units, is just proportional to the point-point susceptibility  $\chi_q$  written as *the* susceptibility  $\xi(\mathbf{k})$  for short:

$$I_{SRO}(\mathbf{k}) = \chi(\mathbf{k}) = N k_B T G_{11}(\mathbf{k}) \quad (51)$$

In the Bragg-Williams (BW, mean field) approximation, valid at very high temperatures, Eq. (51) yields the well-known Krivoglaz-Clapp-Moss (KCM) formula with

$$G_{11}(\mathbf{k}) = 2V(\mathbf{k}) + k_B T/c(1-c) \quad (52)$$

in which  $V(\mathbf{k})$  is the Fourier transform of the effective pair interactions defined previously. In the KCM approximation  $G_{11}(\mathbf{k})$  is just the Fourier Transform of the second-order term in the Taylor's expansion of the free energy. By analogy, Eq. (52) for the general case, may also be written in KCM form

$$\chi(\mathbf{k}) = N k_B T / \Phi(\mathbf{k}) \quad (53)$$

with  $\Phi = G_{11}^{-1}$  representing the Fourier transform of a generalized free energy second derivative. As will be explained in more detail in Sect. 3.2,  $\Phi(\mathbf{k})$  must have symmetry dictated by that of the crystal's point symmetry group and the translational symmetry of the reciprocal lattice. Hence, for any crystallographic space group,  $\Phi(\mathbf{k})$  can be written in symmetry adapted form, as a sum of trigonometric terms multiplied by parameters  $\Phi_s$  calculated from the free energy second derivatives. As an example, for crystals of cubic symmetry class, the expansion is:

$$\Phi(\mathbf{k}) = \Phi_0 + \sum_s \Phi_s \Phi^{(s)}(\mathbf{k}) \quad (54)$$

where  $\Phi^{(s)}$  are "coordination shell functions"

$$\begin{aligned} \Phi^{(s)}(\mathbf{k}) = \frac{z_s}{6} \sum_{j=1}^3 \cos(2\pi h_1 p_j^s) [\cos(2\pi h_2 p_{j+1}^s)] \cos(2\pi h_3 p_{j+2}^s) \\ + \cos(2\pi h_3 p_{j+1}^s) [(\cos 2\pi h_2 p_{j+2}^s)] \end{aligned} \quad (55)$$

where  $z_s$  is the coordination number for shell  $s$ ,  $p_j^s$  are integers and half-integers denoting the Cartesian coordinates of a point in the first octant of shell  $s$ , and  $h_i (= k_i a_i^*/2\pi)$  denote Cartesian coordinates in the first BZ,  $a_i^*$  being reciprocal lattice parameters. The subscripts on direct space coordinates must be taken as  $(j-1)$  modulo  $3 + 1$ . By analogy with  $V(\mathbf{k})$  itself, these parameters  $\Phi_s$  may then be regarded as effective, temperature-dependent pair interactions. An interesting and unexpected consequence of this temperature dependence was recently discovered by Solal et al.<sup>19</sup>

As emphasized by Sanchez, in a remarkable paper<sup>20</sup>, Eq. (53) for  $\chi(\mathbf{k})$  is exact. Unfortunately, for all but the simplest one and two-dimensional Ising models, no exact expression is known for the free energy, hence the matrix  $F(\mathbf{k})$ , and consequently  $G_{11}(\mathbf{k})$  can only be calculated for approximate models. One consequence is that the integration of  $\chi(\mathbf{k})$  over the Brillouin zone will not be a conserved quantity. For the one-dimensional Ising chain with nearest-neighbor interaction, for which the CVM expression is exact, the integrated  $\chi$  does remain rigorously constant with temperature. For two and three-dimensional cases, integrated  $\chi$ , according to various CVM approximations, tends to increase without limit near the instability temperature  $T_0$ , although the temperature variation is less drastic than that for the KCM approximation. As shown elsewhere<sup>21</sup>, SRO intensity maxima appear to be sharper in the CVM than in the KCM approximation..

### 3.2. Special Point Symmetry

As pointed out by Lifshitz<sup>22</sup> many years ago, symmetry-dictated extrema must be found, for any function, at points where  $k$ -space symmetry elements intersect at a point, provided that the function, say  $V(\mathbf{k})$ , possesses the symmetry of the crystal. At these

special points (SP), the so called: "Lifshitz criterion" is satisfied. Later, Khachatryan<sup>23</sup> showed how ordered structures could be constructed from SP ordering waves in fcc and bcc lattices. The role of SP waves in stability theory was then examined by the present author<sup>9,10</sup>, again for the case of fcc and bcc crystals.

It was shown by Haas<sup>24</sup> then by Hornreich, Lubhan and Shtrichman<sup>25</sup> that second order transitions need not occur exclusively for ordering k-vectors located right *at* the SP: the free energy second derivative could present a saddle point at the lowest SP so that actual minima may be located at some distance away but still definitely associated with the SP. In fact, the term "Lifshitz point" was coined<sup>25</sup> to designate the point in phase diagram space at which the free energy second derivative ceases to have a minimum at the SP and just begins to develop the saddle. Thus, at the Lifshitz point, at least one of the eigenvalues of the matrix of spatial second derivatives of the free energy second derivative (with respect to ordering wave amplitudes) vanishes. "Beyond" the Lifshitz point, minima will develop symmetrically about the SP at a k-space distance  $q$ , let us say, from  $k_0$ . It follows that the actual ordering instability can be represented by the ordering wave  $k_0$  amplitude-modulated by a wave of wavelength  $2\pi/q$ . These ideas are described in detail by Takeda et al.<sup>27</sup> and applied to instabilities created by electron irradiation in CuPd samples. The notion of a metastable Lifshitz point is introduced.

From the foregoing, it follows that it is desirable to determine the SP for crystal structures of interest, and to determine the nature of the extrema (maximum., minimum, saddle point) at each SP, for various ranges of energy parameters. This determination was performed, in the BW framework, first for fcc and bcc lattices<sup>24</sup>, then for general crystal structures<sup>26</sup>. In the general case, the recipe for finding the set of SP for any one of the 230 crystallographic space groups is the following one: introduce a center of inversion (if absent) into the symmetry point group  $G_x$  of the crystal, from which the point group  $G_p$  is derived. One then forms the direct product group

$$G_s = G_p \times \{g\} \quad (56)$$

where  $\{g\}$  is the translational group of the reciprocal lattice. The resulting  $G_s$  must then be one of the 24 centered symmorphic groups, i.e. those containing a center of inversion but no glide planes or screw axes. The SP are found by locating the relevant  $G_s$  in the International Tables for Crystallography<sup>27</sup> and noting those Wyckoff positions with fixed coordinates. A complete list of all SP is given in Table 1. Since the translation groups are in k-space, the symmorphic groups are listed for reciprocal space. Actually, it was pointed out by F. Ducastelle, at the conference itself, that, in the case of multiple lattice systems (such as hcp), the scheme just described may produce extraneous "special" points. It is thus necessary to test whether gradients really do vanish at each special point found.

For each group, the origin 000 is always a SP and corresponds to an infinite wave instability. Such an instability would normally give rise to *spinodal decomposition*, as originally described by Cahn<sup>28</sup>. By extension, instabilities associated with other SP will give rise to *spinodal ordering*<sup>9,10</sup>.

For a given crystal, which of the listed SP will actually be a *minimum*, and thus give rise to some spinodal-type reaction, will depend on the nature of the  $V(k)$  in particular on the relative values of the effective pair interactions,  $V_1, V_2, V_3...$  which, in general, may depend on temperature, as mentioned above, as well as on concentration. If these variations are not too abrupt, it is expected that, in rather extensive regions of phase diagram (T,c) space, a given SP instability will predominate. Equilibrium superstructures found in those regions will then be associated with the corresponding SP instability, i.e. will be said to be members of the *SP family of superstructures*. Members of the family can be further subdivided into two classes, (a) those for which the structure factor spectrum



consists exclusively of SP wave vectors (not necessarily *minimum* SP) and (b) those for which the spectrum contains  $k$  vectors located elsewhere in the BZ. The former, SP-structures, were discussed by Khachatryan<sup>23</sup> for fcc and bcc parent lattices, but do not necessarily correspond to lowest energy states. The latter, non-SP-structures, were determined as true ground for restricted sets of  $V_n$  interactions for fcc, bcc and hcp parents<sup>29,30,31</sup>.

In an actual phase diagram, phases other than ordered superstructures may, of course, be found at equilibrium. These compounds, not manifestly related to either fcc, bcc or hcp parents, may be regarded, in a sense, as "interlopers". Examples are A15,  $\sigma$ , Laves... phases.

In any case, the concept of SP families of ordered superstructures is an important one for classifying crystal structures in alloy systems; it is a particularly useful one when attempting to perform first principles calculations.

### 3.3. Example: Instabilities in the Perovskite Basal Plane

Thus far, the treatment has been rather formal. It is thus instructive to consider an example: that of ordering of filled and empty oxygen sites in the Perovskite basal plane, chosen for reasons mentioned in the Introduction.

The plane in question is shown in Fig. 1.<sup>32</sup>

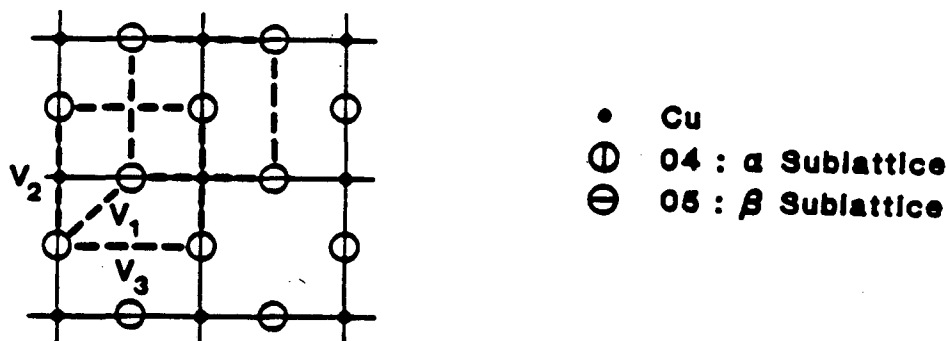


FIGURE 1. Oxygen sublattices on perovskite basal plane with indicated effective pair interactions. Large open circles denote oxygen sites, small filled circles denote Cu atoms.

The open circles represent two types of oxygen sites, occupying two interpenetrating sublattices,  $\alpha$  and  $\beta$ , say. The small filled circles represent the cations, here referred to as Cu atoms because of the relevance of this model to the high- $T_c$  superconductor  $YBa_2Cu_3O_x$ , with  $6 \leq x \leq 7$ . We now introduce three effective pair interactions  $V_r$  defined, following Eq. (36), as

$$V_r = \frac{1}{4} \left[ V_r(O-O) + V_r(\square-\square) - V_r(O-\square) \right] \quad (57)$$

The strongest interaction is expected to be the nearest-neighbor one,  $V_1$ , which couples the two sublattices. It is also necessary to include two second-neighbor-interactions,  $V_2$  which is mediated by the Cu ion, and  $V_3$  which is not. Both  $V_2$  and  $V_3$  connect sites on the same sublattice as shown in Fig. 1. The signs and strengths of the effective pair interactions will, of course, depend on the electronic structure of the full three-dimensional crystal. We adopt the usual convention that  $V_r > 0$  favors "ordering" of the  $r^{\text{th}}$  pair (unlike site occupation), and  $V_r < 0$  favors "clustering" (like-site occupation). We may then perform an ordering stability analysis of the 2D Ising problem by formally expanding the

free energy to second order in the configuration variables as was done in Sect. 3.1. In a mean-field approximation (Bragg-Williams) the configuration entropy is site diagonal in the configuration variables so that all structural effects are determined by the pair interaction term written in its most general form as<sup>26</sup>

$$\Phi = \frac{1}{2} \sum_{m'} \sum_{mm'} v(\mathbf{R}_m + \rho_n - \mathbf{R}_{m'} - \rho_{n'}) \sigma(\mathbf{R}_m + \rho_n) \times \sigma(\mathbf{R}_{m'} - \rho_{n'}) \quad (58)$$

where  $\mathbf{R}_m$  designates a lattice vector and  $\rho_n$  a position inside the unit cell. The interaction parameters depend on the distance between lattice sites and the configuration variables  $\sigma$  denote site occupancy, i.e., +1 is filled, -1 is empty. The summations extend over all pairs of sites, compatible with the limited range of interactions  $v$  considered. The correspondence between these interactions and the  $V_1$ ,  $V_2$ , and  $V_3$  introduced above is established in Fig. 1.

The quadratic form (58) must now be diagonalized. The Fourier diagonalization in Sect. 3.1. was performed under the tacit assumption of translational invariance of all points  $p$  in the reference state. In the present case of interpenetrating lattices, this is no longer the case. Translational symmetry can be restored to the interactions, however, by converting  $v$  to a matrix of elements  $v_{nn'}$ ,<sup>26</sup> the order of the matrix being equal to the number of sublattices considered, here equal to two. Hence, the diagonalization proceeds very much as in Eqs. (47) and (48) except that now the indices ( $n, n'$ ) denote sublattices rather than clusters ( $q, q'$ ) as in Sect. 3.1.

The first step in the diagonalization thus gives

$$\Phi = \frac{1}{2} \sum_{mm'} \sum_{nn'} v_{nn'}(\mathbf{R}_m - \mathbf{R}_{m'} - \rho_{n'}) \sigma_n(\mathbf{R}_m) \sigma_{n'}(\mathbf{R}_{m'}) \quad (59)$$

The second step consists of a lattice Fourier transform over  $N$  sites of a suitably large region:

$$\Phi = \frac{N}{2} \sum_{\mathbf{k}} \sum_{nn'} V_{nn'}(\mathbf{k}) \sigma_n(\mathbf{k}) \sigma_{n'}(-\mathbf{k}) \quad (60)$$

in which  $V_{nn'}(\mathbf{k})$  is the Fourier transform of the effective pair interactions,  $v_{nn'}$ , and  $\sigma_n(\mathbf{k})$  is the amplitude of an "occupancy wave" on sublattice  $n$ . In the third step, the diagonalization is completed by defining "normal modes"  $\Gamma(\mathbf{k})$

$$\sigma_n = \sum_{n'} U_{nn'} \Gamma_{n'} \quad (61)$$

where  $U$  is a unitary matrix diagonalizing  $V$ . Let the eigenvalues of  $V$  be  $\Lambda_n$ . The fully diagonalized expression is thus

$$\Phi = \frac{N}{2} \sum_{\mathbf{k}} \sum_n \Lambda_n(\mathbf{k}) |\Gamma_n(\mathbf{k})|^2 \quad (62)$$

As explained in Sect. 3.2., symmetry-dictated extrema of  $V_{nn'}(\mathbf{k})$ , or of  $\Lambda_n(\mathbf{k})$ , must be located at the special points. In the present case, the group  $G_s$ , defined by Eq. (56), is the two-dimensional square  $p4m$  with fixed-coordinate Wyckoff positions at  $\langle 00 \rangle$ ,

$\langle 1/2 0 \rangle$ , and  $\langle 1/2 1/2 \rangle$ . The short range of interactions postulated for the problem precludes the existence of minima away from the SP, hence the search for k-space minima will be limited to those three points.

The Fourier transforms of the interaction parameters are given by

$$\begin{aligned} V_{11}(\mathbf{k}) &= 2V_2 \cos 2\pi h_1 + 2V_3 \cos 2\pi h_2 \\ V_{22}(\mathbf{k}) &= 2V_3 \cos 2\pi h_1 + 2V_2 \cos 2\pi h_2 \end{aligned} \quad (63)$$

$$V_{12}(\mathbf{k}) = V_{21}(\mathbf{k}) = 2V_1 [\cos \pi(h_1 + h_2) + \cos \pi(h_1 - h_2)]$$

In these equations, the  $V_r$  parameters are those defined in Fig. 1.

At the SP, the eigenvalues take on very simple forms:

$$\begin{aligned} \langle 0 0 \rangle: \quad \Lambda_{\pm}(0 0) &= 2(V_2 + V_3) \pm 4|V_1| \\ \langle 1/2 0 \rangle: \quad \lambda_{\pm}(1/2 0) &= \pm 2|V_2 - V_3| \\ \langle 1/2 1/2 \rangle: \quad \lambda_{\pm}(1/2 1/2) &= -2(V_2 + V_3) \end{aligned} \quad (64)$$

In the search for minimum eigenvalues, only the upper sign needs to be considered. Depending on the relative values of  $V_1$ ,  $V_2$ , and  $V_3$ , one SP eigenvalue will be lower than the other two. Let us divide Eqs. (64) through by  $V_1$  and define normalized interaction parameters

$$x = V_2/V_1 \quad \text{and} \quad y = V_3/V_1$$

These parameters can then be used as coordinates in an "ordering instability map" which indicates the regions in interaction parameter space where a given SP wave will be most unstable. Boundaries between such regions are obtained by equating different SP eigenvalues. The resulting map is shown in Fig. 2 for the case  $V_1 > 0$ .

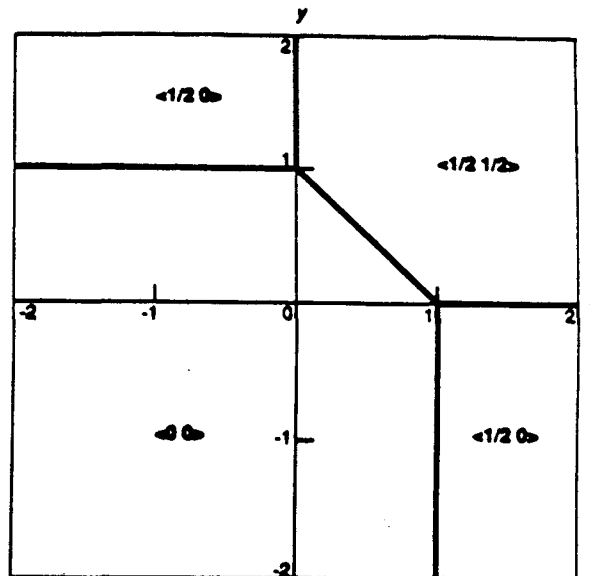


FIGURE 2. Ordering instability map for  $V_1 > 0$ . Coordinates are ratios  $x = V_2/V_1$ ,  $y = V_3/V_1$ .

It is seen that the  $\langle 0 0 \rangle$  instability is favored for "ordering" first-neighbor and "clustering" second-neighbor interactions. Conversely, the  $\langle 1/2 1/2 \rangle$  instability is favored by large "ordering" second-neighbor interactions, and  $\langle 1/2 0 \rangle$  is favored by  $V_2$  and  $V_3$  differing in sign.

When a given "ordering wave" (that with lowest eigenvalue) becomes unstable, the corresponding normal mode amplitude will increase, thereby modulating the sublattice site occupation. Since the normal mode  $\Gamma_+$  (corresponding to  $\Lambda_+$ ) will always have lowest energy, we have by Eq. (61), with  $\Gamma_- = 0$ ,

$$\begin{aligned}\sigma_1(\mathbf{k}) &= u_{11}(\mathbf{k}) \Gamma_+(\mathbf{k}) \\ \sigma_2(\mathbf{k}) &= u_{21}(\mathbf{k}) \Gamma_+(\mathbf{k})\end{aligned}\tag{65}$$

where  $u_{11}$  and  $u_{21}$  are the components of the eigenvector corresponding to  $\Lambda_+(\mathbf{k})$ . At the  $\langle 0 0 \rangle$  SP, the eigenvectors are

$$[u_{11}, u_{21}] = \frac{1}{\sqrt{2}} [1, -\text{Sgn}(V_1)], \quad \text{Sgn}(V_1) = |V_1|/V_1 \tag{66}$$

For the Brillouin zone center instability, infinite-wavelength modulations will be placed on the  $\alpha$  and  $\beta$  sublattices; for  $V_1 > 0$  the two waves will be out of phase, i.e., there will be maximum concentration of filled sites on one sublattice and minimum on the other. For  $V_1 < 0$ , the two waves will be in phase. In the former case, the resulting structure, for average concentration of filled sites,  $c_0 = 1/2$  ( $x=7$  in  $\text{YBa}_2\text{Cu}_3\text{O}_x$ ), will produce the unit cell depicted in the lower left quadrant of Fig. 3a. This structure, with two-dimensional space group symbol  $p2mm$ , is characterized by O-Cu-O...chains along the  $b$  axis and produces the three-dimensional orthorhombic structure  $Pmmm$  of the superconducting phases.

For the zone boundary instabilities  $\langle 1/2 0 \rangle$  and  $\langle 1/2 1/2 \rangle$  intra-sublattice modulations are produced, leading to doubling and quadrupling of the original unit cell,

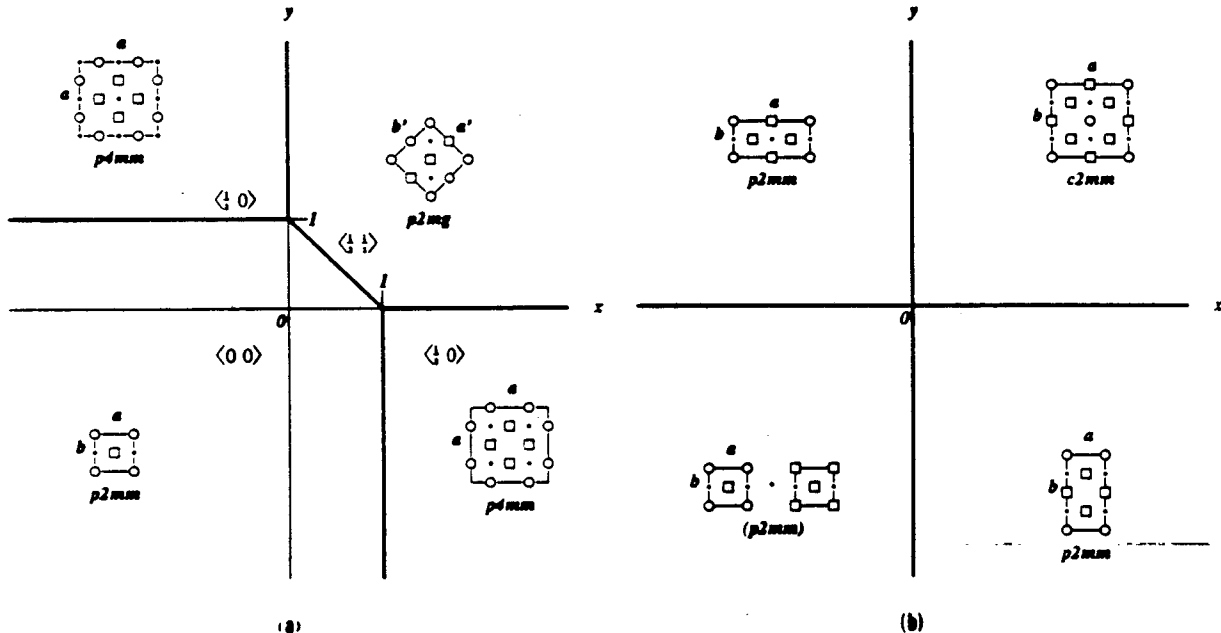


FIGURE 3. Ground states as a function of parameter ratios  $x=V_2/V_1$ ,  $y=V_3/V_1$  at oxygen concentrations (a)  $c_0=0.50$ , (b)  $c_0=0.25$ .

respectively. For both cases, due to the vanishing of the off-diagonal element  $V_{12}(\mathbf{k})$ , the eigenvectors are  $[1,0]$  and  $[0,1]$ . Hence, by Eq. (9), we have for the  $\langle 1/2 0 \rangle$  case,  $\sigma_1(\mathbf{k}) = \Gamma_+(\mathbf{k})$ ,  $\sigma_2(\mathbf{k}) = 0$ . The resulting structure may be interpreted as consisting of one sublattice modulated by a  $\langle 1/2 0 \rangle$  wave, with the other sublattice containing a random distribution of filled and empty sites. Actual ground state structures corresponding to this SP instability will be described in the next Section. For the  $\langle 1/2 1/2 \rangle$  case (for compositions near  $c_0 = 1/2$ ), since  $\Lambda_+ = \Lambda_-$ , both sublattices will be modulated by a  $\langle 1/2 1/2 \rangle$  wave, producing a structure with  $[1,1]$  rows populated alternately by filled and empty sites.

By a fortunate coincidence, the day before I presented, at the Crete meeting, an early version of the above stability analysis (later corrected by Dr. L. T. Wille), Dr. G. Van Tendeloo<sup>33</sup> presented electron diffraction and microscopy results which indicated the existence of a "cell doubling" ordering reaction evidenced by diffuse intensity at point  $\langle 1/2 0 \rangle$  in the high- $T_c$  superconductor. It was thus highly gratifying to see that such a simple analysis could predict actual structures in such complex materials.

#### 4. PHASE DIAGRAMS

The exciting possibility now exists of deriving equilibrium phase diagrams virtually from first principles. The subject is now in its infancy but already some interesting results have been obtained. The CVM has proved to be a reliable tool for performing the required statistical thermodynamics, but requires as input, of course, the structure-independent energy  $E_0^\circ$  of Eq. (39) and the effective clusters interactions  $E_\alpha^\circ$ , defined in Eq. (40), in particular, the effective pair interactions (EPI)  $V_r$  defined in Eq. (36). Several schemes have been proposed recently for calculating the EPI's by quantum mechanical means. A brief summary of these techniques has been given elsewhere<sup>34</sup>.

The calculation of phase diagrams proceeds in two main steps: firstly, equilibrium crystal structures are determined at zero absolute temperature; secondly, equilibria between those structures are determined as a function of temperature. The first problem, one of energy minimization, can itself be subdivided into one of comparing total energies of dissimilar structures, such as fcc and bcc, or intermetallics  $L1_2$  and  $A15$ , for example, at the same concentration, and one of determining ground states of order based on a given fixed lattice. It is this second sub-problem which is addressed in the next section (4.1), and was already alluded to at the end of Sect. 3.2.

The problem of thermodynamic equilibria at non-zero temperatures is to be solved by minimizing the relevant *free* energy. This is where the CVM comes in, as will be briefly described in Sect. 4.2.

##### 4.1. Ground States of Order

Given a fixed lattice (or sublattice), two types of "atoms" (say), and a set of parameters  $V_r$  representing interactions between neighboring atoms, what will be the atomic arrangements ( $\sigma$ ) minimizing the "ordering energy", that given by Eq. (10)? Such is the ground state problem. Thus, the problem is formulated simply, but, except in the simplest of cases, cannot be solved rigorously or completely. A very thorough description of the ground state problem has been given by Finel<sup>13</sup>. Here, only a brief summary will be given.

In Eq. (17), the partial trace  $\rho_\beta$  was expressed as a function of the correlations  $\xi_\alpha$ . In this equation,  $\beta$  represents a cluster of  $n_\beta$  points and the indicated summation is over all subclusters  $\alpha$  contained in  $\beta$ . In highly symmetric structures, several subclusters ( $\alpha$ ) may be crystallographically equivalent, in which case they will have the same correlation

function  $\xi_\alpha$ . All such clusters will be members of a class  $j$ , say, and denoted by  $\alpha_j$ . It is then advantageous to group such clusters into a single term in the summation. Thus, the subcluster summation in Eq. (17) is now replaced by a sum over cluster classes  $j$ ;

$$\rho_\beta(\sigma_\beta) = \rho_\beta^0 \left[ 1 + \sum_j W_j(\sigma_\beta) \xi_j \right] \quad (67)$$

with

$$W_j(\sigma_\beta) = \sum_{\alpha_j} \Phi_{\alpha_j}(\sigma_\beta) \quad (68)$$

In the last equation, the cluster functions  $\Phi$ , for given class  $j$ , differ by nature of the site occupancies  $\sigma_\beta$ . The latter cluster configurations can also be listed in some suitable order, and given an index  $k$ , say. The  $W_{jk}$  may then be considered as elements of a (generally rectangular) matrix, denoted here as *configuration matrix* [for historical reasons, this matrix is often called the "V-matrix," an unfortunate nomenclature since it has nothing to do with the  $V_r$  interaction parameters].

Equation (67) is the practical one used in CVM codes. It has its use in the ground state problem as well: since  $\rho_\beta$  represents a cluster probability, or concentration, for configuration  $\sigma_\beta$ , it must be a non-negative quantity. Hence, the following inequalities must hold

$$\sum_j W_j(\sigma_\beta) \xi_j \geq -1 \quad (69)$$

These inequalities, along with the conditions  $-1 \leq \xi_j \leq +1$  define a convex region in multidimensional  $\xi$ -space (configuration space), the so called *configurational polyhedron*, which contains all realizable configurations  $\sigma$  on the given lattice. It can be shown<sup>13</sup> that the vertices of the polyhedron determine, in principle, all ordered ground states for the given *range* or cluster interactions, different ordered states being stable for different stoichiometries and different ratios of interaction parameters. Unfortunately, except for the case of short-range interactions, inequalities (69) often result in "non constructible crystal structures," which means that the set of inequalities is incomplete, the constraints "too loose." How many more inequalities must one seek to obtain correct ground states? That, unfortunately, appears to belong to a class of mathematically undecidable problems<sup>35</sup>. In simple cases, the problem can be solved in a straight-forward manner; an example, that leading to the ordering maps of Fig. 3, will be discussed in Sect. 4.3.

#### 4.2. Phase Diagram Constructions

In elementary treatments of binary (A,B) phase equilibrium, the common tangent construction is used to derive (or at least to rationalize) phase diagrams. In the present case of free energies which are function of a great many independent variables, the common tangent construction is not appropriate. For this reason, Kikuchi<sup>36</sup> proposed a method of phase equilibrium determination based on minimizing what he called the *grand potential* defined by

$$\omega = f - \mu \xi \quad (70)$$

where  $\xi$  is actually a normalized sum of point correlation variables over the various sublattices and where  $\mu$  is an appropriate chemical potential, shortly to be specified. In Eq. (70),  $f$  is the free energy (30) normalized to one lattice point. The grand potential or free energy minimization proceeds by solving the set of simultaneous non-linear algebraic

equations (28) which, through Eq. (17), are implicit in the linearly independent correlation variables  $\xi$ . To make the meaning of Eq. (70) more explicit, consider a new function  $f_A$  defined as the free energy  $f$  in which  $(2x_A - 1)$  [when  $x_A$  is the average concentration of A atoms] has been substituted for  $\xi_1$ , all of the other  $\xi$  variables having their equilibrium values. Another function  $f_B$  is defined similarly. The classical "intercept rule" may be then written in two alternate ways:

$$\mu_A = f - x_A \frac{df_A}{dx_A} \quad , \quad (71a)$$

$$\mu_B = f - x_B \frac{df_B}{dx_B} \quad , \quad (71b)$$

where also

$$\frac{df_A}{dx_A} = \mu_A - \mu_B = - \frac{df_B}{dx_B} \quad (72)$$

in which  $\mu_A$  and  $\mu_B$  are the classical potentials of A and B respectively. Making use of Eq. (72) and summing Eqs. (71a) and (71b), we obtain immediately Eq. (70), where  $\omega$  now appears as a sum and  $\mu$  as a difference of chemical potentials:

$$\omega = \frac{\mu_A + \mu_B}{2} \quad , \quad \mu = \frac{\mu_A - \mu_B}{2} \quad (73)$$

Calculations of phase equilibrium then proceeds as follows: for fixed values of temperature  $T$  and chemical potential  $\mu$ , the grand potential  $\omega$  is minimized with respect to the independent  $\xi$  variables, the free energy  $f$  to be used being the CVM free energy appropriate for the ordered (or disordered) phase under consideration, i.e. the one for which the  $W$ -matrix reflects the proper sublattice structure. Next, the minimum values of  $\omega$  are plotted as a function of  $\mu$  for that phase and for other phases of interest. Points at which two  $\omega$  vs.  $\mu$  curves intersect determine phase equilibrium. The lowest intersections found are then used to construct the phase diagram: an intersection between curves for phases  $\alpha$  and  $\beta$ , say, yields two values of  $\xi$ , hence, two values of equilibrium concentrations  $x^\alpha$  and  $x^\beta$ , for example, at the chosen temperature. Two sets of all other correlation variables are also obtained, one set for each phase, thereby completely determining the state of order of each of the two phases in equilibrium. This procedure is repeated for all temperatures and for all ordered phases predicted by the ground state analysis. The calculated loci of phase boundary points, in  $T$ - $x_B$  or  $T$ - $\mu$  space constitutes the required *coherent* (or *ordering*) equilibrium phase diagram.

The grand potential method is obviously equivalent to the traditional one since, at a point of intersection of  $\omega$  curves, both the sum  $\omega$  and the difference  $\mu$  of chemical potentials are the same, hence the chemical potentials themselves are equal in the two phases, as required. It is also seen that the grand potential can be obtained from the free energy  $f$  by a Legendre transformation,  $\mu$  which then appears as the intensive (field) variable conjugate to the extensive (density) variable  $\xi$ .

CVM phase equilibria with fixed values of the ratio  $V_2/V_1$  of second to first neighbor pair interactions were explored systematically for the fcc<sup>4,5,6,38</sup> and bcc<sup>37</sup> lattices (for which the ground state problem had been solved exactly, for this range of pair interactions). In practice, EPI's are expected to vary with concentration, due to the influence of both electronic structure<sup>39</sup> and elastic effects<sup>40,41</sup>. Furthermore, pure components A and B may be stable in fcc, bcc, hcp or other crystal structures. The

procedure for calculating a phase diagram should therefore include the following steps: select a lattice (fcc, say), then calculate free energy curves (actually, grand potential curves  $\omega$ ) for that lattice and its relevant ordered superstructures, based on ground state analysis. Repeat the calculation for other disordered state structures (bcc, hcp...) and all of their relevant superstructures. Finally, combine all grand potential curves, at various temperatures, and seek lowest curve intersections; plot intersections in temperature-concentration space. For completeness, a liquid free energy curve should also be included. This can be done by empirical means. This general procedure was followed in a recent calculation<sup>42</sup> of the Ti-Rh phase diagram; the competition between fcc and bcc lattices and their respective superstructures was well illustrated in this example. "Interloper" intermetallic phases (A15...) have not yet been incorporated into the computational scheme.

#### 4.3. Example: Vacancy Ordering in $\text{YBa}_2\text{Cu}_3\text{O}_x$

In Sect. 3.3, a stability analysis of O- $\square$  ordering in the basal Perovskite plane was presented. Such an analysis does not yield ordered ground states readily: One must instead proceed as was described in Sect. 4.1. In the simple case under consideration here, which is that modeled by Fig. 1, it actually suffices to perform a "brute force" calculation as follows: all possible configurations of filled and empty oxygen sites are tested on a 2x2 and a 2x4 lattice containing 8 and 16 oxygen sites, respectively<sup>43</sup>. Structures are then sought which minimized the Hamiltonian

$$\Phi = \frac{1}{2} \sum_P [V_1 \sum_{P_1} \sigma_P \sigma_{P_1} + V_2 \sum_{P_2} \sigma_P \sigma_{P_2} + V_3 \sum_{P_3} \sigma_P \sigma_{P_3}] \quad (74)$$

where  $\sigma = \pm 1$ , according to whether a site is filled or empty. In Eq. (74),  $p$  denotes any lattice site, and  $p_1, p_2, p_3$  denote sites which are respectively nearest and next nearest ( $p_2$ , across a Cu atom;  $p_3$  otherwise) neighbors to it.

With the range of interactions considered, only two stoichiometric compositions gave rise to ordered ground states:  $c_o = 0.50$  and  $c_o = 0.25$  (or 0.75). The resulting structures are indicated in the ordering map of Fig. 3a and 3b for these two concentrations, respectively. Minimum energy structures are designated by their two-dimensional space group symbols. For  $c_o = 0.5$ , the ground state regions are separated by limits (heavy lines) which agree with those found in the stability analysis, Fig. 2. The structure of the orthorhombic superconducting phase is that found in the lower left region of Fig. 3a and clearly results from the  $\langle 0, 0 \rangle$  instability described earlier. In other regions, 2x2 and  $\sqrt{2} \times \sqrt{2}$  structures are predicted.

At stoichiometry  $c_o = 0.25$ , the ordering map regions coincide with the four quadrants of the  $(x, y)$  plane [recall that  $x = V_2/V_1$ ,  $y = V_3/V_1$ ,  $V_1 > 0$ ]. It is seen that phase separation is predicted in the  $(-, -)$  quadrant, cell quadrupling is predicted in the  $(+, +)$  quadrant, and two similar (yet distinct) cell doubling structures are predicted in the other quadrants. In particular, the structure which doubles the  $x$  direction is precisely the one observed by electron microscopy by Zandbergen et al.<sup>33,44</sup> and believed to be that identified by Cava et al.<sup>45</sup> as having a superconducting transition of about 60K.

The next step in the study of vacancy ordering is to formulate a CVM approximation of the free energy. For that, appropriate clusters must be chosen. That aspect of the problem was, until recently, something of a black art. Now, thanks to the work of Schlijper<sup>12</sup> and Finel<sup>13</sup>, significant progress has been made.



At the Crete NATO Institute, Finel gave a special seminar on his method, the detailed exposition of which can be found in his Doctoral dissertation<sup>13</sup>. It is clear from the formulation of Sect. 2.2 that the CVM approximation is based upon the replacement of a density matrix  $\rho$ , for an infinite system (thermodynamic limit), by products of "reduced densities"  $\rho_\alpha$  pertaining to small clusters. The resulting factorization is not expected to be exact (if it were, the three dimensional Ising model would be solved!) but at least it should be required to produce approximate density matrices such that they belong to a class defined by  $\text{Tr } \rho = 1$ . Finel shows how one may use this criterion in selecting appropriate cluster approximations, the first step being that of reducing by unity the number of infinite dimensions of the system.

In the present case, consider again the Perovskite basal plane in the  $p2mm$  arrangement (orthorhombic phase) shown in Fig. 4a. A motif (Fig. 4b) is selected and is translated over the actual structure (Fig. 4a) in such a way that the whole infinite plane is covered. It is seen that there are just four non-equivalent positions of the motif on the two-dimensional structure: two large centered squares (full lines), one on the  $\alpha$ , the other on the  $\beta$  sublattice, and two smaller squares, outlined by dashed lines. For the approximation chosen (motif in 4b), these are the four basic clusters required in this CVM approximation. Of course, the motif could be made larger, presumably ensuring higher accuracy, but at the cost of greatly increased numerical complications.

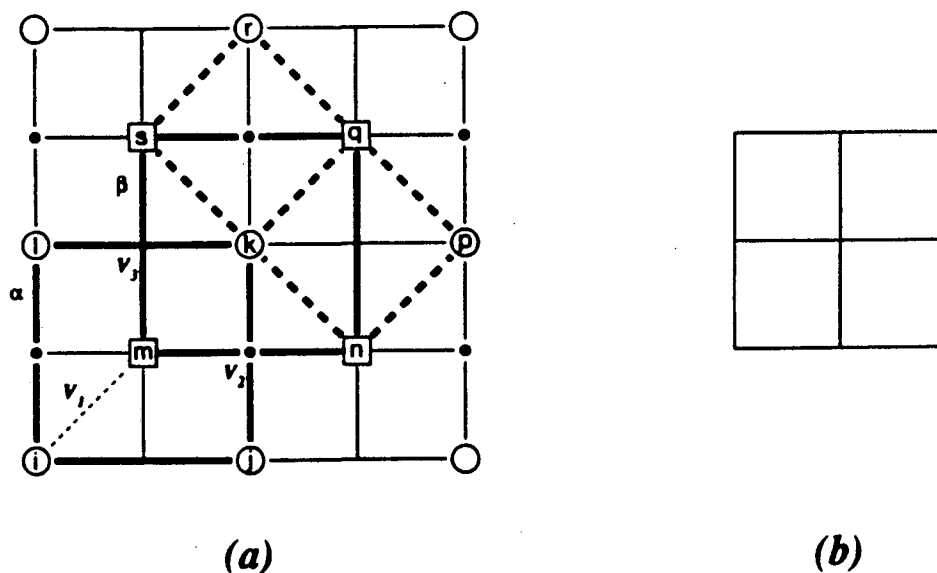


FIGURE 4a. Perovskite basal plane in the orthorhombic phase. As in Fig. 1, but now open circles denote oxygen atoms, and squares denote empty sites. Sites are labeled in accordance to W-matrix notation of Table III. Fig. 4b. is CVM motif.

In principle, all subclusters of the basic ones must be considered. In fact, only a certain number will appear in the entropy formula. To derive the latter, it is merely required to determine the coefficients  $a_\alpha$  appearing in Eqs. (25) to (30). In practice, it is simpler to determine a completely equivalent set of integers, the "Kikuchi-Barker coefficients," obtained from the  $a_i$  (the index  $i$  now stands for a cluster type, or class, consisting of all  $\alpha$  which are equivalent under the symmetry operations of the crystal) by the formula<sup>11</sup>

$$\gamma_i = m_i a_i \quad (75)$$

where  $m_i$  is the number of  $i$ -type cluster per lattice site. The following recursive method<sup>2</sup> is then used to find successive coefficients, starting from the one corresponding to the basic cluster(s) labeled I:

$$\gamma_I = -m_I$$

$$\gamma_i = -m_i - \sum_{j=i+1}^I m_i^j \gamma_j \quad (76)$$

To obtain the Kikuchi-Barker coefficients, it suffices to consider cluster types in the disordered state. In the various ordered states, cluster types split into subclasses, but the  $\gamma_i$  coefficients remain the same (except for a common multiplicative factor). Cluster types in the completely disordered state, with Cu atoms discarded, are listed in Table I












$i$	Cluster	$m_i$	$j=$	1	2	3	4	5	6	7	8	9	10	11	$\gamma_i$	
0		1		1	2	2	2	3	3	3	4	4	4	5	0	
1		2			1	0	0	2	2	0	4	3	0	4	-2	
2,3		2				1	0	1	0	2	2	2	4	4	0	
4		2					1	0	1	1	0	1	2	2	0	
5		4						1	0	0	4	2	0	4	4	
6		2							1	0	0	1	0	2	0	
7		4								1	0	1	4	4	0	
8		1										1	0	0	-1	
9		4											1	0	4	0
10		1												1	1	0
11		1													1	-1

Table I. Cluster type (in the disordered state), number of these per unit cell ( $m_i$ ) and  $m_i^j$  coefficients required to derive Kikuchi-Barker coefficients  $\gamma_i$  according to Eq. (76).

along with the values of  $m_i$  and  $m_i^j$ . The  $\gamma_j$ , calculated by application of Eq. (76), are given in the last column. Many of these  $\gamma_j$  vanish, which could have been predicted from general rules<sup>11,13</sup>. The set of  $\gamma_i$ , leading to the required entropy formula, had been derived earlier by Kikuchi<sup>46</sup>, Kulik<sup>47</sup> and Finel<sup>13</sup>.

How clusters and subclusters split in the ordered orthorhombic (p2mm) phase is indicated, as an example, in Table II. For illustration, Table III gives the explicit form of











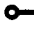















i	$\alpha$	$\beta$	i	$\alpha$	$\beta$
0					
1			6		
2			7		
3			8		
4			9		
5			10		
5'			11		

Table II. Cluster types required for the orthorhombic (p2mm) structure.

$x_1(i,m) = \frac{1}{4}[1 + i\xi_0^\alpha + m\xi_0^\beta + im\xi_1]$
$x_5^\alpha(i,l,m) = \frac{1}{8}[1 + (i+l)\xi_0^\alpha + (m)\xi_0^\beta + (im+lm)\xi_1 + (il)\xi_2^\alpha + (ilm)\xi_5^\alpha]$
$x_8^\alpha(k,r,s,q) = \frac{1}{16}[1 + (k+r)\xi_0^\alpha + (s+q)\xi_0^\beta + (ks+rs+rq+qk)\xi_1 + (kr)\xi_2^\alpha + (sq)\xi_2^\beta + (krs+krq)\xi_5^\alpha + (ksq+rsq)\xi_5^\beta + (krsq)\xi_8^\alpha]$
$x_{11}^\alpha(i,j,k,l,m) = \frac{1}{32}[1 + (i+j+k+l)\xi_0^\alpha + (m)\xi_0^\beta + (im+jm+km+lm)\xi_1 + (il+jk)\xi_2^\alpha + (ij+kl)\xi_3^\alpha + (ik+jl)\xi_4^\alpha + (ilm+jkm)\xi_5^\alpha + (ijm+klm)\xi_5^\alpha + (imk+jml)\xi_6^\alpha + (ijl+ijk+lki+lkj)\xi_7^\alpha + (ijlm+ijkm+lkim+l kjm)\xi_9^\alpha + (ijkl)\xi_{10}^\alpha + (ijklm)\xi_{11}^\alpha]$

Table III. Cluster Probabilities  $x$  (or partial densities  $\rho$ ) for orthorhombic phase expressed as linear functions of correlation variables  $\xi$ , according to Eq. (67).

Eq. (17) for the  $p2mm$  (superconducting) phase, more precisely, of the symmetry adapted from (67), the coefficients of the correlation functions  $\xi$  (corresponding to the clusters of Table II) yielding the elements of the configuration matrix  $W$ . In Table III, only one example each of cluster concentrations  $x_5$ ,  $x_8$  and  $x_{11}$  are given. Other cluster formulas (for  $x_5^\beta$ ,  $x_5^\alpha$  ...), as required by Table II, can be derived similarly, with the help of Fig. 4a.

The resulting phase diagram<sup>48</sup>, obtained from this cluster scheme according to the methods described above is shown in Fig. 5 for the particular choice  $V_1 > 0$ ,  $V_2/V_1 = V_3/V_1 = -0.5$ . The values of these parameters were chosen so that comparisons could be made with diagrams obtained by Monte Carlo simulation<sup>49</sup> and renormalization group methods<sup>50,51</sup>.

At low concentrations and high temperatures, the two-dimensional disordered phase  $4mm$  (short symbol, long space group symbol is  $p4mm$ ) of square symmetry is calculated to be the stable one. It corresponds to the three-dimensional tetragonal phase  $P4/mmm$ . A line of second-order transitions (heavy dashed line) separates the disordered phase region from that of the ordered phase  $mm$ . The upper ordering critical point at stoichiometry  $c_0 = 0.5$  lies at a reduced temperature  $kT_0/V_1 = 4.03$ ; whereas high-temperature series expansions<sup>52</sup> give the value  $kT_0/V_1 = 3.80$ .

The line of second-order transitions ends at a tricritical point (t) which has coordinates  $kT_t/V_1 = 1.41$ ,  $c_0 = 0.19$ , and  $\mu = 3.94$ , where the field variable  $\mu$  represents a difference of

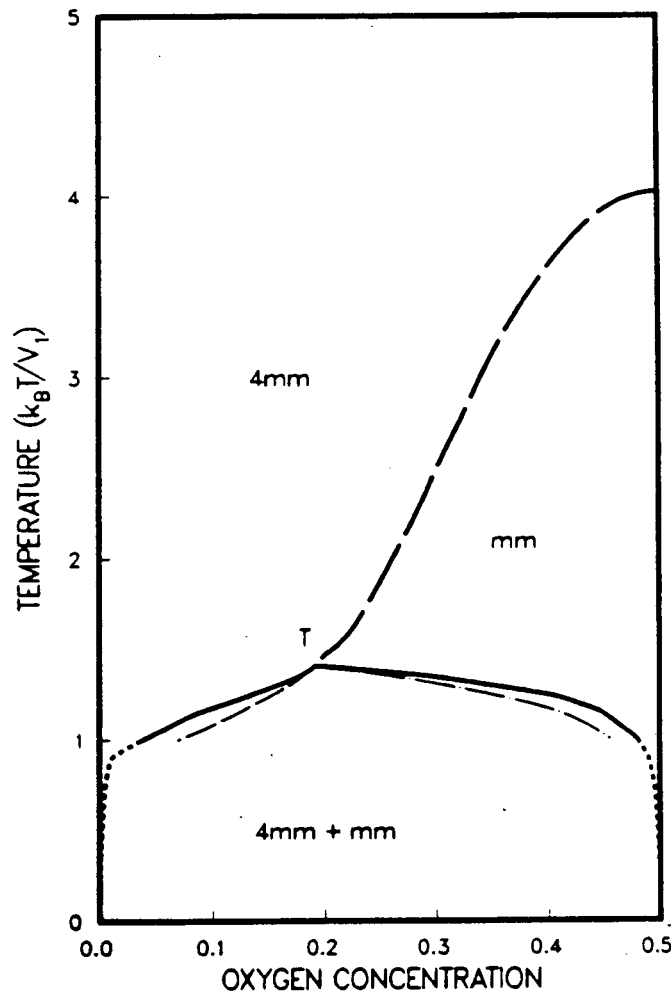


FIGURE 5. CVM phase diagram calculated for  $V_1 > 0$ ,  $V_2 = V_3 = -0.5V_1$ . Tetragonal and orthorhombic phase regions are designated by symbols  $4mm$  (full symbol  $p4mm$ ) and  $mm$  (full symbol  $p2mm$ ), respectively.

chemical potentials  $\mu_O - \mu_{\square}$ . These values are to be compared to those obtained from renormalization group techniques by Rikvold et al.<sup>51</sup>:  $kT_t/V_1 = 1.205 \pm 0.003$ ,  $c_0 \approx .30$ ,  $\mu/V_1 = 3.965 \pm 0.001$  and by Claro and Kumar<sup>50</sup>:  $kT_t/V_1 = 1.28$ ,  $c_0 \approx .31$ , in reasonable agreement with Monte Carlo results<sup>49</sup>. An "interface method" calculation by Slotte<sup>53</sup> gives, for the tricritical temperature,  $kT_t/V_1 \approx -2.27V_2$  at  $\mu/V_1 = 4$ .

Detailed calculations of phase boundary lines in the immediate vicinity of the tricritical point indicate that properties derived by Allen and Cahn<sup>54</sup> on the basis of the Landau theory are well obeyed here: the disordered phase boundary joins the line of second-order transitions with no change in slope, unlike the case for the ordered phase boundary at point  $t$ . The fine dashed line is the metastable extension of the line of second-order transitions and represents an ordering spinodal<sup>9</sup>, i.e. a line below which the disordered phase becomes marginally unstable to small-amplitude ordering fluctuations. The fine dot-dash curve is the locus of marginal instability for phase separation on the partially filled oxygen sublattice. In terms of the stability analysis presented above, the fine dashed curve is the stability limit for two  $\langle 0 \ 0 \rangle$  ordering waves operating, in phase opposition, on the two square sublattices of oxygen sites, and the dot-dash curve is the stability limit for a single  $\langle 0 \ 0 \rangle$  wave acting on the partially filled sublattice in the ordered phase. The two-phase region ( $4mm + mm$ ) rapidly spreads out as the temperature is lowered so that, at absolute zero, the solubility of  $O$  in the disordered phase and  $\square$  in the ordered phase are nil.

These tangency rules and spinodals are mean-field features and are therefore not strictly valid from an equilibrium statistical mechanical standpoint. In practice, however, the spinodal concept is a very useful one as it provides simple interpretations of phenomena observed under the constraint of slow kinetics at low temperatures. In two dimensions, tricritical points are expected to have non-classical exponents<sup>55</sup>, however, so that, in fact, the two-phase coexistence curve at  $t$  should be very flat, as calculated by renormalization group methods, and not pointed, as shown in Fig. 5.

This calculation was presented as a tutorial in the setting up and use of the CVM in an easy-to-visualize two-dimensional example. The case treated is also a very topical one, of course, since it pertains to the high- $T_c$  superconductor  $YBa_2Cu_3O_z$ . Phase diagrams for those interesting cases, with  $V_2 \neq V_3$ , have now been calculated<sup>55</sup>, and show good agreement with experimental findings.

## 5. CONCLUSION

The CVM, though it is a classical approximation, and thus frowned upon by the critical phenomena specialists, has proved itself to be extremely useful, particularly in the area of phase diagram calculations. The method is by no means foolproof, the choice of correct clusters still being more in the nature of an art than a science. Numerical convergence for large-cluster approximations also can be a serious problem, particularly at low temperatures.

Still, the improvement over the standard mean field (Bragg-Williams) methods are so considerable that it is becoming feasible to derive certain classes of phase diagrams from first principles. For that, of course, it will be necessary to calculate physical parameters, such as the EPI ( $V_T$ ), along with structural energies, by quantum mechanical methods. Much progress in this aspect of the problem is being realized currently, and I hope to be able to report on this important topic in the near future.

## 6. ACKNOWLEDGEMENTS

I am indebted to colleagues who have contributed very significantly to the work reported in this paper. Among many others, I should cite the following: Ryo Kikuchi, who taught me the CVM, Juan Sanchez who extended it, Alphonse Finel and Patrice Turchi, both from the research group of François Ducastelle in Paris, who collaborated on CVM and electronic band structure calculations, along with Marcel Sluiter. Also, Luc Wille corrected an earlier version of the perovskite stability analysis and, along with Arjun Berera, performed the  $\text{YBa}_2\text{Cu}_3\text{O}_x$  phase diagram calculations. Early CVM work was funded, in part, by the U.S. Army Research Office (Durham). Current research on phase diagrams calculations is supported by a grant from the Director, Office of Energy Research, Materials Sciences Division, U.S. Department of Energy, under contract DE-AC03-76SF00098.

## REFERENCES

1. R. Kikuchi, *Phys. Rev.* **81**, 988 (19851).
2. J. A. Barker, *Proc. Roy. Soc., A* **216**, 45 (1953).
3. J. Hijmans and J. de Boer, *Physica* **21**, 471, 485, 499 (1955).
4. J. M. Sanchez and D. de Fontaine, *Phys. Rev. B* **17**, 2926 (1978).
5. J. M. Sanchez and D. de Fontaine, *Phys. Rev. B* **21**, 216 (1980).
6. J. M. Sanchez and D. de Fontaine, *Phys. Rev. B* **25**, 1759 (1982).
7. R. Kikuchi, *J. Chem. Phys.* **60**, 1071 (1974).
8. D. M. van Baal, *Physica (Utrecht)* **64**, 571 (1973).
9. J. M. Sanchez, D. Gratias and D. de Fontaine, *Acta Cryst. A* **38** (1982) 214.
10. D. de Fontaine, "Configurational Thermodynamics of Solid Solutions", in *Solid State Phys.*, H. Ehrenreich, F. Seitz and D. Turnbull, Eds., Vol. 34, pp. 73-294, Academic Press (1979).
11. J. M. Sanchez, F. Ducastelle and D. Gratias, *Physica (Utrecht)* **128A**, 334 (1984).
12. A. Schlijper, *J. Stat. Phys.* **35**, 285 (1984); **40**, 1 (1985).
13. A. Finel, *Thèse de Doctorat d'Etat*, Université Pierre et Marie Curie, Paris (1987), unpublished.
14. T. Morita, *J. Phys. Soc. Jpn.* **12**, 753, 1060 (1957); *J. Math. Phys.* **13**, 115 (1972).
15. F. Ducastelle, *J. Phys. C* **8**, 3297 (1975).
16. F. Ducastelle and F. Gautier, *J. Phys. F* **6**, 2039 (1976).
17. C. Sigli and J. M. Sanchez, *CALPHAD* **8**, 221 (1984).
18. A. Gonis, G. M. Stocks, W. H. Butler and H. Winter, *Phys. Rev. B* **29**, 555 (1984).
19. F. Solal, R. Caudron, F. Ducastelle, A. Finel and A. Loiseau, *Phys. Rev. Lett.* (in press).
20. J. M. Sanchez, *Physica (Utrecht)*, **111A**, 200 (1982).
21. T. Mohri, J. M. Sanchez and D. de Fontaine, *Acta Metall.* **33**, 1463 (1985).
22. E. M. Lifshitz, *J. Phys. USSR* **7**, **61**, 251 (1942).
23. A. G. Khachatryan, *Phys. Status Solidi B* **60**, 9 (1973).
24. C. Haas, *Phys. Rev. A* **140**, 863 (1965).
25. R. M. Hornreich, M. Lubhan and S. Shtrikman, *Phys. Rev. Lett.* **35**, 1678 (1975); *Phys. Rev. B* **19**, 3799 (1979).
26. J. M. Sanchez, D. Gratias and D. de Fontaine, *Acta Cryst. A* **38**, 214 (1982).
27. International Tables for Crystallography, Vol. A, Space Group Symmetry, T. Hahn, ed., Kluwer Acad. Publisher (1987).
28. J. W. Cahn, *Acta Metall.* **9**, 795 (1961).
29. J. Kanamori, *Prog. Theor. Phys.* **35**, 16 (19866); J. Kanamori and M. Kaburagi, *J. Physique (Paris)* **38**, C7, 274 (1977).

30. S. M. Allen and J. W. Cahn, *Acta Metall.* **20**, 423 (1972); *Scripta Metall.* **7**, 1261 (1973).
31. T. Kudo and S. Katsura, *Progr. Theor. Phys.* **56**, 435 (1976).
32. D. de Fontaine, L. T. Wille and S. C. Moss, *Phys. Rev. B* **36**, 5709 (1987).
33. G. Van Tendeloo, H. W. Zandbergen and S. Amelinckx, *Sol. St. Comm.* **63**, 603 (1987).
34. D. de Fontaine, M. Sluiter and P. Turchi, *Proc. Phase Transformations Conference*, Cambridge, UK, 6-10 July, Institute of Metals (in press).
35. A. Schlijper, private communication.
36. R. Kikuchi and D. de Fontaine, NBS Special Publication No. 496, G. C. Carter, ed., p. 967 (1978).
37. T. Mohri, J. M. Sanchez and D. de Fontaine, *Acta Metall.* **33**, 1171 (1985).
38. M. Sluiter, P. Turchi, Fu Zezhong and D. de Fontaine, *Physica (Utrecht)*, (in press).
39. P. Turchi, M. Sluiter and D. de Fontaine, *Phys. Rev. B* **36**, 3161 (1978).
40. L. G. Ferreira, A. A. Mbaye and A. Zunger, *Phys. Rev. B* **35**, 6475 (1987).
41. K. Terakura, T. Oguchi, T. Mohri and K. Watanabe, *Phys. Rev. B* **35**, 2169 (1987).
42. M. Sluiter, P. Turchi, Fu Zezhong and D. de Fontaine, *Phys. Rev. Lett.* (in press).
43. L. T. Wille and D. de Fontaine, *Phys. Rev. B* **37** (1988).
44. H. W. Zandbergen, G. Van Tendeloo, T. Okabe and S. Amelinckx, *Physica Status Solidi (a)*, (in press).
45. R. J. Cava, B. Batlogg, C. H. Chen, E. A. Rietman, S. M. Zahurak and D. Werger, *Phys. Rev. B* **36**, 5709 (1987).
46. R. Kikuchi (private communication).
47. J. Kulik (unpublished and at U.C. Berkeley).
48. A. Berera, L. T. Wille and D. de Fontaine, *J. Stat. Phys.* (in press).
49. K. Binder and D. P. Landau, *Phys. Rev. B* **21**, 1941 (1980).
50. F. Claro and V. Kumar, *Surf. Sci.* **119**, L371 (1982).
51. P. A. Rikvold, W. Kinzel, J. D. Gunton and K. Kashi, *Phys. Rev. B* **28**, 2686 (1986).
52. J. Oitmaa, *J. Phys. A: Math. Gen.* **14**, 1159 (1961).
53. P. A. Slotte, *J. Phys. C: Sol. St.* **16**, 2935 (1983).
54. S. M. Allen and J. W. Cahn, in "Alloy Phase Diagrams," L. M. Bennett, T. B. Massalski and B. C. Giessen, eds., *Materials Res. Soc. Proc.* **19**, 195 (1983).
55. J. W. Wheeler (private communication).

*LAWRENCE BERKELEY LABORATORY  
TECHNICAL INFORMATION DEPARTMENT  
UNIVERSITY OF CALIFORNIA  
BERKELEY, CALIFORNIA 94720*